INTERNATIONAL JOURNAL FOR NUMERICAL METHODS IN FLUIDS
Int. J. Numer. Meth. Fluids 2006; **50**:911–924
Published online 31 October 2005 in Wiley InterScience (www.interscience.wiley.com). DOI: 10.1002/fld.1085

Redesign of a sharp heel draft tube by a validated CFD-optimization§

B. D. Marjavaara*,† and T. S. Lundström‡

Division of Fluid Mechanics, Luleå University of Technology, SE-97187 Luleå, Sweden

SUMMARY

Numerical optimization techniques in flow design are often used to find optimal shape solutions, regarding, for instance, performance, flow behaviour, construction considerations and economical aspects. The present paper investigates the possibilities of using these techniques in the design process of a hydropower plant. This is realized by optimizing the shape of an existing sharp heel draft tube and validating the result with previously performed experiments. The actual shape optimization is carried out with the response surface methodology, by maximizing the average pressure recovery factor and minimizing the energy loss factor. The result from the optimization shows that it is possible to find an optimal solution on rather coarse grids. The location of the optimum is similar to the experiments, but the improvements are unexpectedly small. This surprising result indicates that the simulated flow field does not completely act as the real flow, which may be a result of the applied inlet boundary conditions, insufficient turbulence models and/or the steady flow assumption. Copyright © 2005 John Wiley & Sons, Ltd.

KEY WORDS: CFD; optimization; response surface methodology; draft tube; diffuser; hydropower

1. INTRODUCTION

Shape optimization for flow design refers here to a numerical procedure to, in some perspective, find an automatic optimized bounding geometry of an industrial fluid flow. The technique has been demonstrated in a number of cases, but several problems have to be solved before it can be routinely applied in product development [1–3]. One problem is that

*Correspondence to: Daniel Marjavaara, Division of Fluid Mechanics, Luleå University of Technology, SE-97187 Luleå, Sweden.
†E-mail: dama@ltu.se
‡E-mail: stlu@ltu.se
§Parts of the article were also presented at the 22nd IAHR Symposium on Hydraulic Machinery and Systems, 29 June–2 July, Stockholm, Sweden, 2004.

Contract/grant sponsor: VINNOVA

Received 14 February 2005
Revised 12 August 2005
Accepted 14 August 2005

Copyright © 2005 John Wiley & Sons, Ltd.

massive computational resources are often required to solve the non-trivial flow equations for several geometries. Others are that the stability of the optimum computed is often unknown and that it is not evident how to choose the best optimization technique. The insufficient physical description of the flow adds to the complexity. Conversely, there are many benefits of a fully working procedure. It will, for instance, be possible to get reliable results in reasonable time, to find new products with better functionality and to save cost and time in product development, maintenance and support. It is therefore vital to further develop, verify and validate efficient shape optimization techniques.

This paper considers a shape optimization of the Turbine-99 draft tube geometry formerly used in two ERCOFTAC Turbine-99 workshops [4–6]. It is a physical 1:11 model of Hölleforsen sharp heel draft tube. The sharp heel construction is representative of designs around 1950, and is a rather odd construction from a flow design perspective. It was basically chosen in order to reduce investment cost. Nevertheless, the efficiency of such a draft tube has been proved to be good. Still, small improvements to the draft tube shape are of importance due to huge production volumes. Several successful experimental investigations have also been performed to redesign these kinds of sharp heel draft tubes into curved draft tubes, showing that it is possible to reduce the hydraulic losses in the draft tube, and thereby increase the overall efficiency of the hydropower plant [7, 8]. Smoothing the sharp heel corner of the Turbine-99 draft tube with a removable curved insert, for example, yields an efficiency improvement in the turbine of about 0.5% for both model and full-scale tests [8]. Note that the actual performance increase in the draft tube is unknown, but the flow field analysis indicates that it is higher than 0.5%. The present shape optimization is done according to this experimental redesign, in order to validate the optimization result and to study how the optimal design is affected by both grid size and grid error. The optimization is performed with the response surface methodology (RSM) and the overall objective is to minimize the hydraulic losses by maximizing the average pressure recovery factor and minimizing the energy loss factor.

2. TECHNICAL APPROACH

A general flow chart for a shape optimization strategy in flow design consists of three stages in the following order: *geometric parameterization*, *computational fluid dynamic* (*CFD*) *simulation and numerical optimization*, see Figure 1. In the first stage an appropriate number of design variables are chosen so that they describe the modifications of the shape of the geometry in a feasible way. The second stage considers the actual CFD calculation, where the first action is to build or modify the geometry based on the values of the design variables from previous iteration. If such results do not exist, initial values have to be set to get a proper initial shape of the geometry. When this is done, the computational grid is generated and the flow equations are solved. The results from the calculations are then sent to the numerical optimization stage, where an objective function and an optimization algorithm have been specified. The optimization evaluation will then result in some new values of the design variables, which in next turn leads to a modification on the shape of the geometry and an additional CFD simulation if the result is inadequate. On the other hand, if the result is satisfactory, an optimum design has been found. Details on these three stages for the draft tube in focus now follow.

Copyright © 2005 John Wiley & Sons, Ltd.

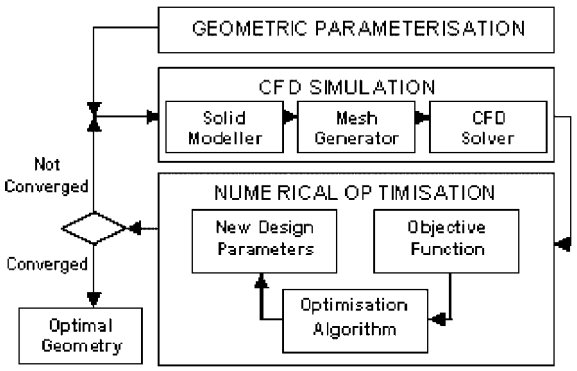

Figure 1. A general shape optimization flow chart.

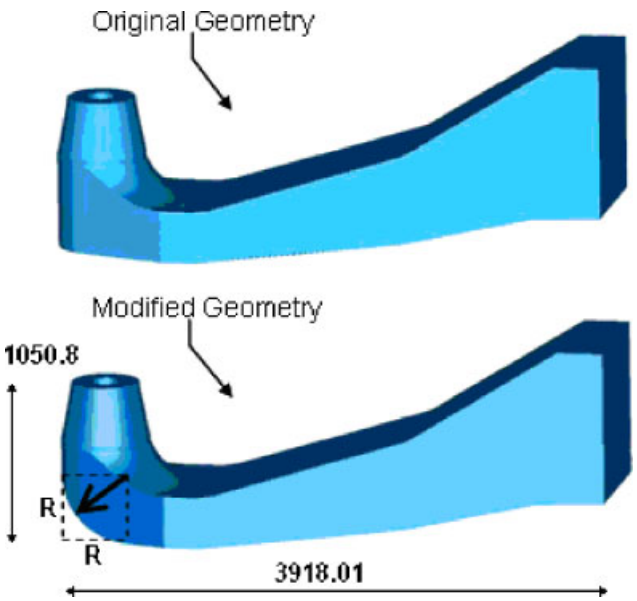

Figure 2. The original ERCOFTAC Turbine-99 draft tube geometry on top and the sharp heel modification of it on bottom (mm).

2.1. *Geometric parameterization*

The main challenge with the *geometrical parameterization* is to find a minimum amount of design variables that cover such as wide a spectrum of shapes as possible. When alterations of the sharp heel region are done according to the experimental redesign presented in Reference [8], the number of design variables are reduced to the radius R of the heel insert, as shown in Figure 2. The actual geometric parameterization and definition of the design variable follows the adapted design parameterization presented in Reference [1], since this method is an appropriate choice when redesigning old constructions. It should, however, be recalled that

Copyright © 2005 John Wiley & Sons, Ltd.

the design variable R is neither the only one nor the best one. It is used here simply to validate the present work with previously successful experimental efficiency improvements studies [7, 8], together with the fact that it is a rather simple, inexpensive and not so time-consuming redesign of an old construction. Changing the inlet cone part of the draft tube will probably give the highest efficiency improvements, since most of the pressure recovery takes place in this portion of the fluid domain. A reconstruction of this part is, however, not straightforward.

2.2. CFD simulation

The commercial CFD code CFX-5 [9] is used to solve the flow in the draft tube, with the assumption of steady, incompressible and turbulent water flow. The solver is a coupled solver, based on the finite volume method on an unstructured grid. It uses shape functions to evaluate the derivates for the pressure gradient term and the diffusion term [9]. The advection term is discretized with a formally second-order accurate scheme (numerical advection correction scheme with a blend factor of 1.0) in the end of the solution progress, for both the continuity and momentum equation as recommended in References [9, 10]. In the beginning of the solution progress, a locally automatic changing scheme between first and second order (high resolution) was chosen to increase the robustness of the solution progress. For the turbulent equations, however, only a first-order scheme is used during the whole solution progress due to robustness problems.

The fluid domain or the actual geometry of the Turbine-99 draft tube is built and modified with the commercial CAD software I-deas NX 10 [11] according to the geometric parameterization discussed earlier. Note that the draft tube geometry is also extended at the outlet so that it follows the provided grid at the second ERCOFTAC Turbine-99 Workshop [4, 6]. This is done to ensure that a constant average static pressure is an acceptable assumption at the outlet of the draft tube.

The computational grid is generated with the commercial structured grid generator ICEM CFD Hexa [12]. To minimize the numerical errors and the effects of differences in the grid topologies, the same grid topology was used for all radii of the heel insert, implying that the generated grids are altered only in the sharp heel corner. This precaution is important since it has been shown that the result of a CFD calculation is closely connected to the topology and quality of the grid, especially at the inlet and the cone of the draft tube [4–6]. To also ensure that the grid topology has as good quality as possible (angles, aspect ratios, etc.), the grid resolutions are non-uniform.

The applied inlet boundary conditions are exactly the same as (regarding velocity components, fluctuations, symmetry assumption, radial velocity assumption, dissipation length scale, etc.) those used for the T-mode in the second ERCOFTAC Turbine-99 Workshop [4, 6, 13]. The experimental efficiency improvements reported here were also conducted for this operational mode [8]. Note that the T-mode represents the optimal operation condition, i.e. measurements from the point with highest efficiency on the propeller curve. During the optimization the inlet profile is kept fixed, although it is probably sensitive to draft tube modifications. In addition, it has been showed that, for example, the radial velocity assumption has a large impact on the draft tube performance [14]. This type of sensitivity analysis of the inlet boundary conditions will, however, not be performed here. At the outlet two zero-pressure conditions are implemented to increase the robustness of the solution progress. To start, an opening boundary condition is used that allows flow into and out of the fluid domain, while toward

Copyright © 2005 John Wiley & Sons, Ltd.

the end and in most of the solution progress an outlet boundary is used that allows only flow out over the boundary. This procedure improves the convergence rate and it minimizes the risk for the solver to fail to find a converged solution.

The turbulence in the draft tube flow is modelled with the standard k–ε model and by usage of scalable wall functions on smooth walls (no-slip) [15]. The arguments for the use of this model are that the main interest is to investigate methods for draft tube optimizations with reasonable CPU usage. It is, however, well known that this turbulence model is unable to predict all details of the flow accurately [16, 17], but it should be mentioned that this model is able to predict the main flow features of the flow in the draft tube [4–6].

2.3. Numerical optimization

For the numerical optimization the target values of the objective function are chosen to be the average pressure recovery factor C_p and the energy loss factor ζ, as indirect indications of the economical gains. Although there are several methods and algorithms to relate the target values to each other, e.g. multi-objective optimization, C_p and ζ will be, respectively, maximized and minimized individually. The average pressure recovery factor C_p is defined as

$$C_p = \frac{\dfrac{1}{A_{\text{out}}} \iint_{A_{\text{out}}} p \, \mathrm{d}A - \dfrac{1}{A_{\text{in}}} \iint_{A_{\text{in}}} p \, \mathrm{d}A}{\dfrac{1}{2}\rho \left(\dfrac{Q_{\text{in}}}{A_{\text{in}}} \right)^2} \tag{1}$$

where A is the area, p is the static pressure, Q is the flow rate, ρ is the density and the subscripts 'in' and 'out' correspond, respectively, to the inlet and the outlet. The energy loss factor ζ is defined as

$$\zeta = \frac{\displaystyle\iint_{A_{\text{in}}} p_{\text{tot}} \mathbf{u} \cdot \mathbf{n} \, \mathrm{d}A + \iint_{A_{\text{out}}} p_{\text{tot}} \mathbf{u} \cdot \mathbf{n} \, \mathrm{d}A}{\displaystyle\iint_{A_{\text{in}}} p_{\text{dyn}} \mathbf{u} \cdot \mathbf{n} \, \mathrm{d}A} \tag{2}$$

where $\mathbf{n}$ is the surface normal vector, p_{dyn} is the dynamic pressure, p_{tot} is the total pressure and $\mathbf{u}$ is the velocity vector.

As optimization algorithm the RSM is chosen. The RSM can in general be described in three phases; design of experiments (DOE), response surface (or polynomial) and optimization phase [3]. In the first phase, a suitable number of points are chosen within or on the borders of a predefined design space so that they reflect the global behaviour of the object function. One frequently used DOE technique is the face centred composite design (FCCD). This technique generates $(2^N + 2N + 1)$ designs points and is common when the total number of design variables N are relatively few. The design points are located at the corners of the design space, the centres of the faces and at the centre of the design space. In the second phase, the response surface phase, a low ordered polynomial (quadratic or cubic) is usually fitted to the DOE points. This response surface approximation is actually a least square problem, so it is computationally straightforward. In the third and final phase, the optimization phase, an optimization algorithm is used to find the optimum point of the response surface, often with a gradient-based algorithm. In this case, the *fminbnd* function in Matlab [18] was selected.

Copyright © 2005 John Wiley & Sons, Ltd.

In the end, the fidelity of the response surface model has to be scrutinized by analysing the value of the coefficient of multiple regression R^2 and/or the adjusted coefficient of multiple regression R_a^2. A value near one is obtained when the fit is acceptable, whereas a lower value should be taken as a sign of a poor fit. Another relevant measure is the root mean square (rms) error σ.

The optimization problem can be summarized as

$$\begin{aligned} &\text{minimize:} \quad f = -C_p \quad \text{and} \quad f = \zeta \\ &\text{subject to:} \quad 10 \leqslant R \leqslant 610\,\text{mm} \end{aligned} \tag{3}$$

where f is the objective function. The lower and upper constraint of R (10 and 610 mm, respectively) in Equation (3) is set by the CAD and grid generation techniques used here. However, it is reasonable to assume that a draft tube with the lower constraint (10 mm) has approximately equal efficiency as the original draft tube, since the radius is rather small.

3. COMPUTATIONAL DETAILS

A total number of 36 CFD simulations were carried out with different coarseness of the grid for the shape optimization and the error estimation. The DOE strategy for the RSM-based shape optimization was evaluated on a modified FCCD technique, where five ordinary points ($2^1 + 2 \times 1 + 1 = 5$) are complemented by one extra point that is designed to evaluate the behaviour of C_p and ζ for small radius R. A non-uniform design point distribution was also chosen, since it is expected that the optimum design point is within a 'small' radius R, according to $R = 10, 60, 110, 210, 410$ and 610 mm. For each radius R, six grids were generated automatically, composed of about 0.6M, 0.9M, 1.3M, 1.7M, 2.3M and 2.7M nodes, respectively. The minimal angle for these grids sizes varied from 22° to 25° depending on the radius and the grid size. The average $y+$ value at near-wall nodes was about 32 (from 1 to 126) for the draft tube wall and about 70 (from 1 to 235) for the runner wall. Regions with low $y+$ values correspond to areas with separated flows, where the velocity goes to zero, and regions with the highest values can be traced to the inlet, runner and cone part of the draft tube, where the velocity gradients are steeper.

Each CFD simulation was assumed converged when all rms residuals had dropped to about 10^{-5}, which is sufficient for most engineering problems according to Reference [9]. The iterative convergence for C_p and ζ was monitored by plotting the iterative error as a function of the rms mass source residual ratio. By doing this, the iterative error could be estimated to 1.8% according to the method presented in Reference [14].

A grid error analysis was carried out for all R based on the three finest grids (2.7M, 2.2M and 1.7M nodes) following the Richardson Extrapolation method presented in Reference [19] and by using C_p and ζ as the dependent variables. However, it turned out that neither the differencing scheme, the extrapolated values nor the grid error could be estimated in a reasonable way. For example, the order of the scheme was often about 10 for C_p and negative for ζ. The reason is that not all the grids are in the asymptotic range, which is exemplified in Figure 3, where the grid error analysis for $R = 10$ and 610 mm with ζ as the dependent variable is shown. The symbols correspond to DOE points, the line to the extrapolated curve and α is the grid refinement factor ($\alpha = 1$ and 1.62 corresponds to the finest and coarsest grid, respectively). Nevertheless, it is still possible to estimate the grid error by using the

Copyright © 2005 John Wiley & Sons, Ltd.

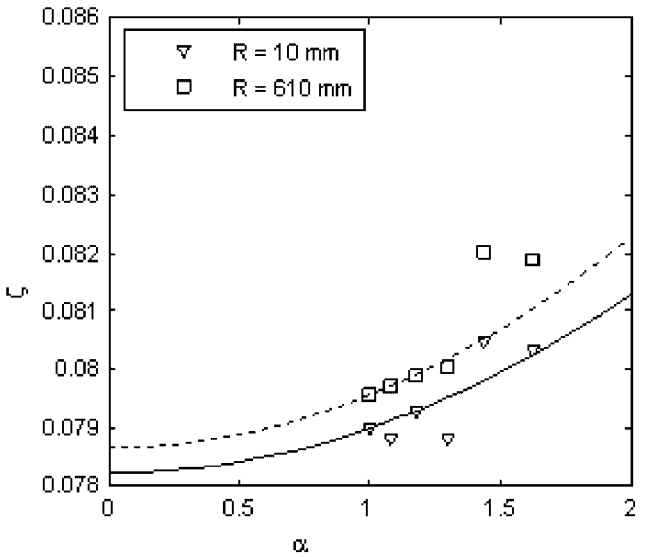

Figure 3. Richardson extrapolation on an assumed second-order scheme for $R = 10$ and 610 mm, with ζ as the dependent variable.

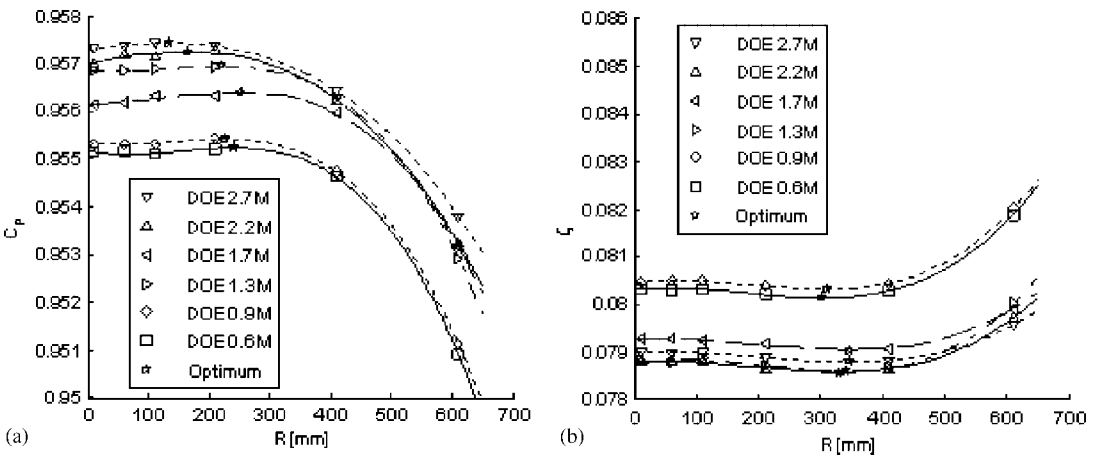

Figure 4. The constructed cubic response surfaces. Symbols correspond to DOE designs, stars to optimal solutions and lines to the response surfaces: (a) C_p; and (b) ζ.

same equations and by assuming that the actual order of the differencing scheme is between one and two [20]. This also implies that only two grids are necessary for the estimation of the grid error. Doing so on grid 2.7M and 1.7M nodes, the grid convergence error can be estimated to about 0.4–0.7% in C_p and to about 1.2–2.6% in ζ for the finest grid and all radii. The 2.2M node grid was excluded in the above calculations since the objective value distributions differ slightly from the two other grids and follow more the behaviour of the three coarsest grids (1.3M, 0.9M and 0.6M nodes). One explanation to this difference is that

Copyright © 2005 John Wiley & Sons, Ltd.

the grid refinement factor used to generate the computational grids is not of equal multiple, forcing the objective value distribution to alter. Thereby, the grids follow different paths in the asymptotic range. Another possible explanation is that the iterative convergence is not fully satisfactory, which is more pronounced for the three finest grids since the grid error becomes smaller.

4. RESULT

4.1. Optimization analysis

The result of the shape optimization showed that a cubic response surface model performed better than a simpler quadratic model on the two objectives, C_p and ζ. For the cubic model, the R^2_a value was high and the σ value was low, indicating that the fits are of high accuracy, see Table I. Also, the behaviour of the cubic models, C_p and ζ as a function of R, was similar for all the six grid sizes, see Figure 4, where the symbols correspond to DOE designs, stars to optimum solutions and lines to the constructed response surfaces models. It is also seen that the estimated optimal solution of R is about 210 mm for C_p and about 330 mm for ζ, see Table II and Figure 4. The values differ as a function of grid size with about 46% for C_p and about 13% for ζ. The large error in C_p can be traced to the scatter of the DOE design point distribution for the two finest grids. To check the reliability of the estimated optimal solution, two additional CFD simulations were performed on the two coarsest grids with the estimated optimal value of R. This showed a remarkable good estimation of the credible optimal value for C_p and for ζ, see Table II. A remark is that all estimated optimum solutions of C_p and ζ estimated an increase in the objective compared to the approximated original design (R equal to 10 mm), see Table II. The most interesting result, however, is the unexpected small improvements of the objective functions C_p and ζ, around 0.02% within the

Table I. Result of the response surface analysis.

	Quadratic response surface					Cubic response surface				
	R^2	R^2_a	σ	Mean	# of terms	R^2	R^2_a	σ	Mean	# of terms
C_p 0.6M	0.97025	0.95042	0.00038	0.95437	6	0.99968	0.99920	0.00005	0.95437	6
C_p 0.9M	0.97552	0.95921	0.00034	0.95454	6	0.99998	0.99994	0.00001	0.95454	6
C_p 1.3M	0.97808	0.96346	0.00030	0.95613	6	0.99999	0.99999	0.00001	0.95613	6
C_p 1.7M	0.97211	0.95352	0.00027	0.95568	6	0.99880	0.99701	0.00007	0.95569	6
C_p 2.2M	0.99520	0.99201	0.00014	0.95636	6	0.99909	0.99772	0.00007	0.95636	6
C_p 2.7M	0.99673	0.99455	0.00011	0.95662	6	0.99998	0.99995	0.00001	0.95662	6
ζ 0.6M	0.94054	0.90090	0.00021	0.08056	6	0.99908	0.99770	0.00003	0.08056	6
ζ 0.9M	0.93389	0.88981	0.00021	0.08072	6	0.99988	0.99969	0.00001	0.08072	6
ζ 1.3M	0.88636	0.81060	0.00023	0.07897	6	0.99535	0.98838	0.00006	0.07897	6
ζ 1.7M	0.89222	0.82037	0.00013	0.07933	6	0.99873	0.99682	0.00002	0.07933	6
ζ 2.2M	0.91371	0.85619	0.00015	0.07890	6	0.99874	0.99684	0.00002	0.07890	6
ζ 2.7M	0.88641	0.81069	0.00012	0.07904	6	0.99793	0.99482	0.00002	0.07904	6

Copyright © 2005 John Wiley & Sons, Ltd.

Table II. Result of the CFD and optimization analysis.

	DOE						Cubic response surface		
	10 (mm)	60 (mm)	110 (mm)	210 (mm)	410 (mm)	610 (mm)	R_{OPT} (mm)	OPT response	OPT CFD
C_p 0.6M	0.95514	0.95517	0.95513	0.95521	0.95464	0.95090	241	0.95525	0.95522
C_p 0.9M	0.95534	0.95532	0.95532	0.95542	0.95474	0.95112	227	0.95542	0.95542
C_p 1.3M	0.95687	0.95686	0.95689	0.95696	0.95630	0.95292	222	0.95696	—
C_p 1.7M	0.95614	0.95620	0.95632	0.95633	0.95598	0.95316	252	0.95641	—
C_p 2.2M	0.95702	0.95719	0.95715	0.95729	0.95624	0.95325	165	0.95727	—
C_p 2.7M	0.95732	0.95738	0.95744	0.95737	0.95643	0.95380	135	0.95744	—
ζ 0.6M	0.08034	0.08031	0.08032	0.08021	0.08028	0.08189	303	0.08013	0.08016
ζ 0.9M	0.08048	0.08050	0.08051	0.08038	0.08044	0.08201	309	0.08031	0.08037
ζ 1.3M	0.07880	0.07877	0.07887	0.07872	0.07865	0.08002	339	0.07859	—
ζ 1.7M	0.07929	0.07930	0.07924	0.07916	0.07908	0.07991	345	0.07904	—
ζ 2.2M	0.07880	0.07880	0.07880	0.07864	0.07864	0.07971	330	0.078570	—
ζ 2.7M	0.07899	0.07897	0.07898	0.07888	0.07882	0.07955	345	0.078795	—

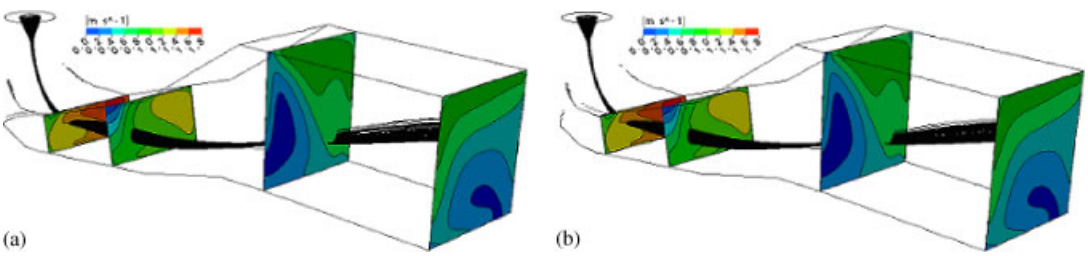

Figure 5. Calculated streamlines from the runner and velocity contour plots: (a) $R = 10$ mm; and (b) $R = 210$ mm.

interval $10 \leqslant R \leqslant 410$ mm. This can be compared to the experimental result that shows an efficiency improvement in the turbine of around 0.5%, and indicating that the improvements of the pressure recovery factor should be even higher than that. Note that the numerically obtained improvement is much smaller than the numerical uncertainties (iterative and grid error). The most likely reason for this is that the physical model, used in the CFD calculations, is not good enough to describe all the flow features in the draft tube. Before discussing this fact let us study the simulated flow field in detail.

4.2. *Flow analysis*

The result of the calculated flow field for all R was similar to what has been derived in other studies [4–6]. It captured among other things regions with separated flow, secondary flow with two main vortices and a vortex rope moving from one side of the draft tube to the other, as shown in Figures 5 and 6. For small R the prediction consistently gave three regions with separated zones: one small beneath the runner cone, a second one in the sharp

Copyright © 2005 John Wiley & Sons, Ltd.

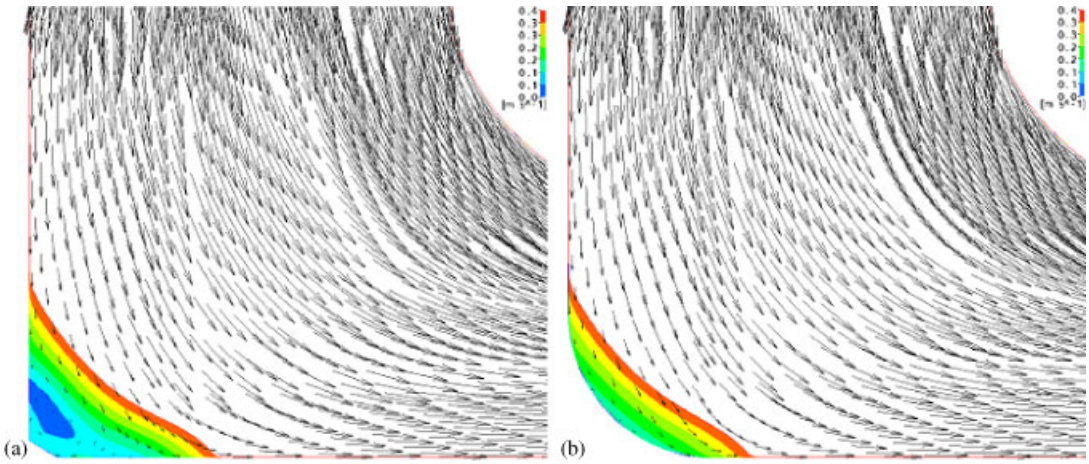

Figure 6. Velocity vector and contour plots at the sharp heel corner: (a) $R = 10\,\text{mm}$; and (b) $R = 210\,\text{mm}$.

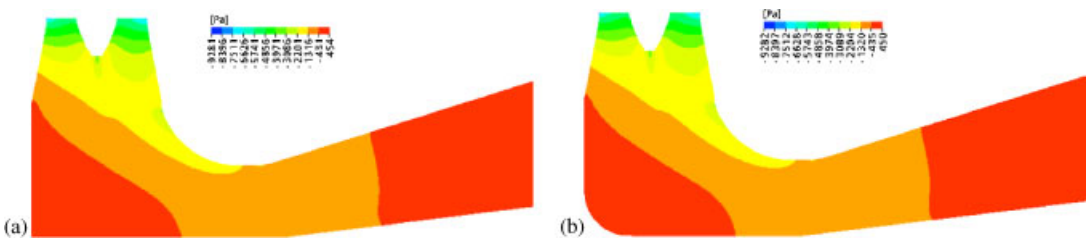

Figure 7. The pressure distribution at a plane through the draft tube: (a) $R = 10\,\text{mm}$; and (b) $R = 210\,\text{mm}$.

heel corner and a third large one at the upper left wall just before the extension at the outlet, seen downstream. For higher R the separation region in the sharp heel corner disappeared as expected, but the efficiency did not increase considerably as mentioned earlier, see Figure 6. This can be due to the fact that an 'artificial wall' is built up by the flow at the optimal R, and therefore C_p and ζ are not influenced until R becomes large enough. In consensus there is no remarkable alteration in the velocity field and the pressure distribution with respect to R, see Figure 7. In fact, the only tendency to a difference in the pressure distribution occurs in the sharp heel corner of the draft tube, compare Figure 8. Here, the pressure recovery is plotted along the normalized upper, respectively, lower wall centre line and the rings correspond to experimental measurements on the original draft tube ($R = 0\,\text{mm}$) reported in Reference [13]. It can then be seen that most of the pressure is recovered in the cone. Also, the inlet radial pressure is independent of R, see Figure 9. The disparities between the obtained radial pressure distribution and the experimental values near the cone wall, as seen in Figure 9, can be traced to the first grid layer adjacent to the wall, suggesting that it is a numerical issue rather than

Copyright © 2005 John Wiley & Sons, Ltd.

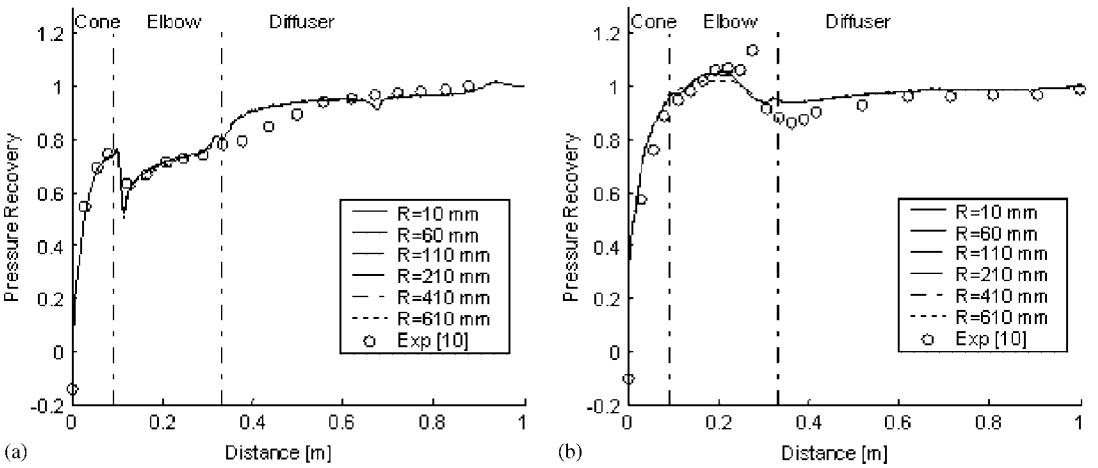

Figure 8. Pressure recovery along the centre line. Lines correspond to CFD simulations and rings to experimental measurements in Reference [10]: (a) upper wall; and (b) lower wall.

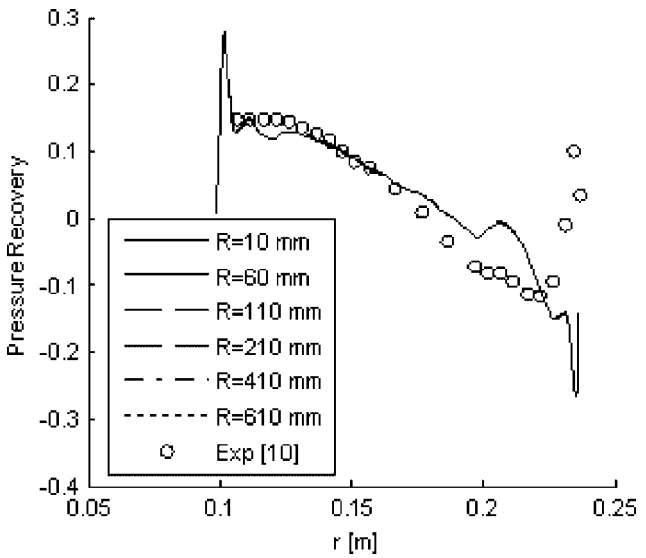

Figure 9. The inlet radial pressure distribution. Lines correspond to CFD simulations and rings to experimental measurements in Reference [10].

a flow feature. This drop in the radial pressure also disappears a few grid layers downstream, suggesting that the inlet must be extended upstream or the runner geometry included in the computation process to obtain reliable values.

Copyright © 2005 John Wiley & Sons, Ltd.

5. DISCUSSION

The calculated simulated flow field is similar to what has previously been obtained, but differs from experimental redesign studies [4–8]. There are at least three possible explanations to the discrepancies between the simulations and the experimental results, all being based on the assumption made on the flow in the CFD calculations. The first explanation is that the flow is assumed stationary although it is obviously transient, leaving many of the strongly impressionable flow features off. Angular resolved inlet data are also available, but have not been used in this study. The second explanation is related to the turbulence model; theoretically, a more advanced turbulence model would predict the flow field more accurately. It should, however, be compared to the fact that the standard k–ε simulations by the participants of the second ERCOFTAC Turbine-99 Workshop predicted the major flow features [4–6]. The third and final explanation is the fact that modifications to the draft tube geometry may also reflect in alterations in the inlet velocity profile, and thereby also the outcome of the CFD calculations, due to the elliptic behaviour of the solved equations [7]. Therefore, the runner geometry should probably be included in the computational processes for the optimization, to get significant efficiency improvements. It is, however, not taken into account here since the inlet velocity profiles are fixed. Three closely connected questions to this last explanation that also can change the result are, the reliability of the symmetry assumption, the radial velocity profile assumption and the tangential velocity profile assumption done here and in the ERCOFTAC Turbine-99 workshops [4–6, 14]. The inlet velocity profile is most likely not symmetric in this case, since it has been shown that the profile is not symmetric in a Francis turbine [21]. For the radial velocity profile in its turn, it has already been shown that it has a large influence on the final result [14]. In fact, the variations of C_p and ζ were larger than those observed in this shape optimization study. In addition, the tangential velocity profile has an alteration in signs near the runner wall, resulting in a huge velocity gradient and requiring a very fine grid resolution near the wall. This change of sign originates from the log wall assumption and the third-order polynomial fitting of the measured tangential velocity profile, whose correctness can be discussed. Finally, it should be recalled that the inlet section of the draft tube is very close to the runner blades, see Figure 2.

6. CONCLUSION

This work demonstrates the potential of a procedure to automatically optimize new or existing parts of the waterways in a hydropower plant. To exemplify, a cubic response surface model performs better than other models when fitted to simulated values. Its general shape is furthermore independent of the grid size although the actual level varies. It also shows an excellent agreement between predicted optimal values and CFD-simulated values at optimal conditions. Hence, for cases where the underlying physical description of the flow field is correct, rather coarse grids can be used to predict the optimal design. However, for the draft tube in focus, the small gains obtained by CFD for the optimal design as compared to experimental results suggest that the physical description of the flow must be enhanced before the evaluated technique can be used more frequently for this type of component improvements. In practice, the major explanations to the relatively small improvements derived by CFD are that: (i) the flow is assumed stationary although it is obviously transient, leaving many of

Copyright © 2005 John Wiley & Sons, Ltd.

the strongly impressionable flow features off; (ii) the k–ε turbulent model is insufficient; and (iii) modifications to the draft tube geometry should reflect in alterations in the inlet velocity profile. Three closely connected questions to this last explanation that also influence the result are, is the reliability of the symmetry assumption, the radial velocity profile assumption and the tangential velocity profile assumption done here and in the ERCOFTAC Turbine-99 workshops [4–6, 14]. An additional remark from this work is that it is of highest importance to monitor the convergence of the objective functions, especially for fine grids, when the iterative error becomes greater than the grid error.

To conclude, the methodology proposed is working very well, but to get reliable and decisive results for the present case the physical description of the flow must be enhanced, since the numerically obtained improvement is much smaller than the experimental improvement and the numerical uncertainties. The way forward is to further enhance the flow modelling capabilities until the accuracy leads to errors less than one order of magnitude of the changes in the objective function(s). Then it is also crucial to define better independent parameters, such that the variations induced on the objective function(s) are one order of magnitude larger than the numerical uncertainties.

ACKNOWLEDGEMENTS

The authors gratefully acknowledge valuable comments and suggestions provided during the work by Professor H. Gustavsson, Dr T. F. Engström and Dr M. J. Cervantes at Luleå University of Technology, Sweden, Mr U. Andersson, Dr P. Andreasson, Dr R. Karlsson and Dr N. Dahlbäck at Vattenfall Utveckling AB, Ålvkarleby, Sweden, and Dr J. Burman at Volvo Aero Corporation, Trollhättan, Sweden. The work was carried out within the Polhem laboratory and was therefore sponsored by VINNOVA and the participating industries.

REFERENCES

1. Marjavaara BD, Lundström TS. Automatic shape optimisation of a hydropower draft tube. *Proceedings of 4th ASME_JSME Joint Fluids Engineering Conference*, vol. 1C, 2003; 1819–1824.
2. Eisinger R, Ruprecht A. Automatic shape optimization of hydro turbine components based on CFD. *TASK Quarterly* 2001; **6**:101–111.
3. Burman J. Geometry parameterisation and response surface-based shape optimisation of aero-engine compressors. *Doctoral Thesis*, vol. 09, Luleå University of Technology, Sweden, 2003; 1–21.
4. *Turbine-99. The IAHR Workshops on Draft Tube Flow*. URL http://www.sirius.ltu.se/strl/Turbine-99/index.htm [cited 30 May 2005].
5. Gebart BR, Gustavsson LH, Karlsson RI. *Proceedings of Turbine-99 Workshop on Draft Tube Flow*, Porjus, Sweden. *Technical Report*, vol. 11, Luleå University of Technology, Sweden, 2000; 1–16.
6. Engström TF, Gustavsson LH, Karlsson RI. *Proceedings of Turbine-99 Workshop 2 on Draft Tube Flow*. URL: http://www.sirius.ltu.se/strl/Turbine-99/t99_2/index_T99w2.htm [cited 30 May 2005].
7. Gubin MF. *Draft Tubes of Hydro-electric Stations*. Amerind Publishing Co.: New Delhi, 1973; 127–145.
8. Dahlbäck N. Redesign of sharp heel draft tube—results from tests in model and prototype. In *Proceedings of XVIII IAHR Symposium on Hydraulic Machinery and Cavitation*, vol. 2, Cabrera E, Espert V, Martìnes F (eds). 1996; 985–993.
9. CFX®. *Version 5.6*, Copyright © 1996–2003, ANSYS Europe Ltd.
10. Casey M, Wintergerste T. Special interest group on quality and trust in industrial CFD: best practice guidelines. *ERCOFTAC* 2000, *Version 1.0*; 11–19.
11. I-deas NX®. *Version 10*, Copyright © 2004, UGS The PLM Company.
12. ICEM CFD®. *Version 5.0*, Copyright © 2004, ANSYS, Inc.
13. Andersson U. An experimental study of the flow in a sharp-heel draft tube. *Licentiate Thesis*, vol. 08, Luleå University of Technology, Sweden, 2000; 1–15.
14. Cervantes MJ, Engström TF. Factorial design applied to CFD. *Journal of Fluids Engineering* 2004; **126**:791–798.

Copyright © 2005 John Wiley & Sons, Ltd.

15. Grotjans H, Menter FR. Wall functions for general applications CFD codes. *ECCOMAS 98 Proceedings of the Fourth European Computational Fluid Dynamics Conference*, 1998.
16. Hanjalic K. Second-moment turbulence closures for CFD: needs and prospects. *International Journal of Computational Fluid Dynamics* 1999; **12**:67–97.
17. Durbin PA, Reif BA. *Statistical Theory and Modeling for Turbulent Flows*. Wiley: New York, 2000; 118–132.
18. MATLAB®. *The Language of Technical Computing*, *Version 7.0.1*, Copyright © 1984–2004. The MathWorks, Inc.: Matick, MA.
19. Celik I, Zhang WM. Calculation of numerical uncertainty using Richardsons extrapolation: application to some simple turbulent flow calculation. *Journal of Fluids Engineering* 1995; **117**:439–445.
20. Bergström J. Approximations of numerical errors and boundary conditions in a draft tube—*Proceedings of Turbine-99 Workshop on Draft Tube Flow*, Porjus, Sweden. *Technical Report*, vol. 11, Luleå University of Technology, Sweden, 2000.
21. Vekve T. An experimental investigation of draft tube flow. *Doctoral Thesis*, vol. 36, Norwegian University of Science and Technology, Norway, 2004; 72–118.

Copyright © 2005 John Wiley & Sons, Ltd.